Stable bright solitons in two-component Bose-Einstein condensates

A. I. Yakimenko,[1,2] K. O. Shchebetovska,[1] S. I. Vilchinskii,[1] and M. Weyrauch[3]

[1]*Department of Physics, Taras Shevchenko National University, Kiev 03022, Ukraine*
[2]*Institute for Nuclear Research, Kiev 03680, Ukraine*
[3]*Physikalisch-Technische Bundesanstalt, Bundesallee 100, D-38116 Braunschweig, Germany*

Two-dimensional fundamental soliton-soliton pairs are investigated in binary mixtures of Bose-Einstein condensates with attractive interactions between atoms of the same type. Both attractive and repulsive interactions between atoms of different types are considered. The general properties of the stationary states are investigated variationally and numerically. The stability regions of the soliton-soliton pairs are determined.

I. INTRODUCTION

Binary mixtures of Bose-Einstein condensates (BECs) are interacting quantum systems of macroscopic scale which exhibit rich physics not accessible in a single-component degenerate quantum gas. The key difference between multicomponent and single-component BECs is the intercomponent interaction. In view of their unique properties binary mixtures of BECs open up intriguing possibilities for a number of important physical applications, including quantum simulation [1], quantum interferometry [2], and precision measurements [3,4].

Various types of nonlinear matter wave structures have been predicted for multicomponent BECs [5–9]. However, many basic properties of two-component BECs remain to be investigated even in simple mean-field approaches based on coupled Gross-Pitaevskii equations (GPEs) with a vector order parameter. Most previous work on two-dimensional (2D) and three-dimensional (3D) vector solitonic structures focused on BECs with repulsive intracomponent interactions [10–14].

Since the scattering length of ^{7}Li atoms is negative, a binary mixture of BECs with attractive intercomponent interactions could be realized experimentally by simultaneously trapping ^{7}Li atoms in different hyperfine states. Experimental progress to control the strength and even the sign of intraspecies and interspecies interactions via Feshbach resonances [15,16] opens new prospects for investigations of attractive BECs. It also motivates recent extensive theoretical studies of two-component matter wave solitons for different signs of intra- and intercomponent interactions (see, e.g., [17–24]).

As is well known, bright 2D and 3D solitons, described by a GPE with attractive nonlinearity, are unstable and may collapse in a finite amount of time, if the number of atoms in the condensate exceeds a critical value (see, e.g., Ref. [25]). Recent theoretical investigations [26] predicted the existence of stable soliton-vortex pairs in trapped BECs with attractive intracomponent interactions. However, the ground-state 2D soliton-soliton structures in such BECs have never been investigated and will be the focus of the present work. Note that in a different context soliton-soliton pairs, described by a similar model, but without linear potential, are found to be unstable [27]. It is reasonable to expect that a stabilization of fundamental vector solitons could occur in an additional external trapping potential.

In the present work we perform a detailed theoretical analysis of nonlinear matter wave structures in binary mixtures

of atoms with attractive intracomponent interactions and attractive as well as repulsive intercomponent interactions. General properties of the steady states of such systems are investigated by means of a variational analysis and numerical simulations. The conditions for the existence and stability of matter wave vector solitons are revealed. Since no experimental work on disk-shaped bright solitons is known to us, we hope that the present study encourages experimental investigations in this direction. Relevant parameters for such experiments can be extracted from the estimation of the critical particle densities given in the following sections.

II. MODEL

We consider a binary mixture of BECs at zero temperature described in mean-field approximation by two coupled Gross-Pitaevskii equations (GPEs) ($j \in \{1,2\}$):

$$i\hbar \frac{\partial \Psi_j}{\partial t} = (\hat{H}_j + g_{jj}|\Psi_j|^2 + g_{j,3-j}|\Psi_{3-j}|^2)\Psi_j, \quad (1)$$

with $\hat{H}_j = -\frac{\hbar^2}{2M_j}\nabla^2 + V_j(\mathbf{r})$, and M_j is the mass of an atom of type j loaded into the axially symmetric harmonic external trapping potential $V_j(\mathbf{r}) = M_j\omega_\perp^2(x^2 + y^2)/2 + M_j\omega_z^2 z^2/2$. Interactions between atoms of the same type (*intra*-component interactions) are characterized by the diagonal coupling coefficients $g_{jj} = 4\pi\hbar^2 a_{jj}/M_j$, where a_{jj} are the s-wave scattering lengths for binary collisions between these atoms. *Inter*-component interactions are controlled by the off-diagonal coupling terms $g_{12} = g_{21} = 2\pi\hbar^2 a_{12}/M_*$ with the reduced mass $M_* = M_1 M_2/(M_1 + M_2)$. Note that our simple mean-field approach provides a reasonable approximation for the evolutionary scenarios investigated here; however, a mean-field approach of course fails at the final stage of the collapse when the atomic density increases catastrophically.

We assume that the longitudinal trapping frequency ω_z is much larger than the transversal trapping frequency $\omega_\perp$ ($\omega_z \gg \omega_\perp$) and that the nonlinear interactions $\sim g_{ij}$ are weak with respect to the confinement strength of the potential in the longitudinal direction. In this case the BEC is "disk shaped" and we may assume that the longitudinal motion of condensates is frozen in $\Psi_j(\mathbf{r},t) = \tilde{\Psi}_j(x,y,t)\Upsilon_j(z,t)$, where $\Upsilon_j(z,t) = (l_{zj}\sqrt{\pi})^{-1/2}\exp(-\frac{i}{2}\omega_z t - \frac{1}{2}z^2/l_{zj}^2)$ is the ground-state wave function of the longitudinal harmonic trapping potential, $l_{zj} = \sqrt{\hbar/(M_j\omega_z)}$. After integrating out the

longitudinal coordinates, the GP equations take the effective 2D form

$$i\frac{\partial \tilde{\Psi}_j}{\partial t} + (\hat{h}_j + |\tilde{\Psi}_j|^2 + b_{j,3-j}|\tilde{\Psi}_{3-j}|^2)\tilde{\Psi}_j = 0, \qquad (2)$$

where $\hat{h}_1 = \Delta_\perp - r^2$, $\hat{h}_2 = \kappa\Delta_\perp - \frac{r^2}{\kappa}$, $\kappa = M_1/M_2$, $r = \sqrt{x^2 + y^2}$, and $\Delta_\perp = \partial^2/\partial x^2 + \partial^2/\partial y^2$ is the 2D Laplacian. Here we have introduced the dimensionless variables $(x,y) \to (x,y)/l_{\perp 1}$, $t \to t/\tau$, and $\tilde{\Psi}_j \to \tilde{\Psi}_j/\sqrt{C_j}$, where $l_{\perp 1} = \sqrt{\hbar/(M_1\omega_\perp)}$, $\tau = 2/\omega_\perp$, $C_j = \hbar\omega_\perp\sqrt{\pi(l_{z1}^2 + l_{z2}^2)}/(2|g_{jj}|)$. Dimensionless coupling parameters are defined by $b_{12} = -\frac{g_{12}}{|g_{11}|}\sqrt{\frac{2}{1+\kappa}}$ and $b_{21} = -\frac{g_{21}}{|g_{22}|}\sqrt{\frac{2\kappa}{1+\kappa}}$. For simplicity, we consider here only the symmetric case $M_1 = M_2$ and $g_{11} = g_{22}$, so that $\kappa = 1$ and $b_{12} = b_{21} = \sigma$. Furthermore, we specifically consider only cases where the diagonal part of the interaction matrix g_{ij} is attractive ($g_{11} < 0$, $g_{22} < 0$) while the off-diagonal terms $g_{12} = g_{21}$ may be attractive ($g_{12} < 0, \sigma > 0$) or repulsive ($g_{12} > 0, \sigma < 0$).

The coupled differential equations given in Eq. (2) have the following integrals of motion: (i) the number of particles in each component

$$N_j = \int |\tilde{\Psi}_j|^2 d^2\mathbf{r}, \qquad (3)$$

(ii) the total energy

$$E = E_1 + E_2 - \sigma \int |\tilde{\Psi}_1|^2 |\tilde{\Psi}_2|^2 d^2\mathbf{r}, \qquad (4)$$

with

$$E_j = \int \left(|\nabla\tilde{\Psi}_j|^2 + r^2|\tilde{\Psi}_j|^2 - \frac{1}{2}|\tilde{\Psi}_j|^4 \right)d^2\mathbf{r},$$

(iii) momentum, and (iv) angular momentum.

III. STATIONARY SOLUTIONS

We consider now stationary vector soliton solutions of the coupled GPEs (2). We are looking for a ground state of the form

$$\tilde{\Psi}_j(\mathbf{r},t) = \psi_j(r)e^{-i\mu_j t}, \qquad (5)$$

where $r = \sqrt{x^2 + y^2}$. Each solution is characterized by chemical potentials μ_j. The real functions $\psi_j(r)$ satisfy the coupled equations

$$\mu_j\psi_j + \psi_j'' + \frac{1}{r}\psi_j' - r^2\psi_j + (\psi_j^2 + \sigma\psi_{3-j}^2)\psi_j = 0 \quad (6)$$

and the boundary conditions $\psi_j'(0) = 0$ and $\psi_j(\infty) = 0$. At fixed strength of the intercomponent interaction σ we then obtain a two-parameter family of vector soliton solutions (with the chemical potentials μ_1 and μ_2 as parameters).

Obviously, vector solitons with the same chemical potential $\mu_1 = \mu_2 = \tilde{\mu}$ and the same radial profiles $\psi_j(r)$ are described by a single GPE with a harmonic potential and an effective interaction strength $\tilde{\sigma} = 1 + \sigma$. It is known (see, e.g., Ref. [28]) that 2D solitonic solutions of this equation exist for $\tilde{\mu} < 2$ if $\tilde{\sigma} > 0$ and for $\tilde{\mu} > 2$ if $\tilde{\sigma} < 0$. The value $\tilde{\mu} = 2$ coincides with the eigenvalue of the ground state of a linear Schrödinger equation with harmonic potential; i.e., nonlinear terms vanish

and the number of atoms tends to zero when $\tilde{\mu} \to 2$. If $\tilde{\sigma} < 0$, the number N of atoms grows rapidly for $\tilde{\mu} > 2$; if $\tilde{\sigma} > 0$, N saturates at a critical value $N_{cr}/\tilde{\sigma}$ where $\tilde{\mu} \to -\infty$. Here, $N_{cr} = 11.68$ is the number of atoms in the fundamental Townes soliton, which is the localized solution of a single GPE without external trap.

Using these results for one-component solitons as a guide, one may expect qualitatively different properties for vector solitons with strong repulsion ($\sigma < -1$) or weak repulsion $-1 < \sigma < 0$. Analogously, we will also discuss separately the properties of the soliton-soliton pairs with weak attraction ($0 < \sigma < 1$) and strong attraction ($\sigma > 1$).

A. Attractive intercomponent interactions ($\sigma > 0$)

The set of equations represented by Eq. (6) was solved numerically by a stabilized relaxation method similar to that described in Ref. [29]. In addition, we performed a variational analysis of the fundamental vector solitons. The variational results not only provide an appropriate initial condition for our numerical relaxation procedure but also they show a good agreement with our numerical results as is seen, e.g., from Figs. 1(b)–1(d) and 1(f)–1(h).

If all interactions between particles are attractive, then both solitonic components are basically bell shaped and a simple trial function of the form

$$\psi_j(r) = \sqrt{\frac{N_j}{\pi a_j^2}}e^{-\frac{1}{2}\frac{r^2}{a_j^2}} \qquad (7)$$

is expected to be a good approximation. Here a_j is the effective width of component j. The trial function is normalized to the number of particles: $\langle\psi_j|\psi_j\rangle = N_j$. Substituting the trial function given by Eq. (7) into Eq. (4), we obtain the energy

$$E = E_1 + E_2 - \sigma E_{12} \qquad (8)$$

with

$$E_j = N_j\left(\frac{1}{a_j^2} + a_j^2 - \frac{N_j}{4\pi a_j^2}\right), \quad E_{12} = \frac{N_1 N_2}{\pi(a_1^2 + a_2^2)}.$$

A soliton solution corresponds to a stationary point of the total energy at a fixed number of particles in each component: $(\partial E/\partial a_1)_{N_1,N_2} = 0, (\partial E/\partial a_2)_{N_1,N_2} = 0$.

Obviously, the two-parameter family of vector soliton solutions is symmetric with respect to the simultaneous interchange $\mu_1 \leftrightarrow \mu_2$ and $\psi_1 \leftrightarrow \psi_2$, so that in the plane of chemical potentials (μ_1,μ_2) the solutions are symmetric with respect to the line $\mu_1 = \mu_2$. To utilize this symmetry we present the number of particles for each component as functions of the difference $\mu_- = \mu_1 - \mu_2$ at the fixed total chemical potential $\mu_+ = \mu_1 + \mu_2$. Typical results are shown in Figs. 1(b)–1(d) and 1(f)–1(h).

Note that the region of existence for vector soliton pairs has boundaries in the (μ_1,μ_2) plane, beyond which only single-component (scalar) solitons exist. For different fixed values of μ_+ we determined the number of particles in each component and then constructed the complete existence region, which is shown in Figs. 1(a) and 1(e). In these figures the solid black line separates the vector solitons from the scalar soliton region where one solitonic component vanishes and the red dashed line indicates the boundary where the
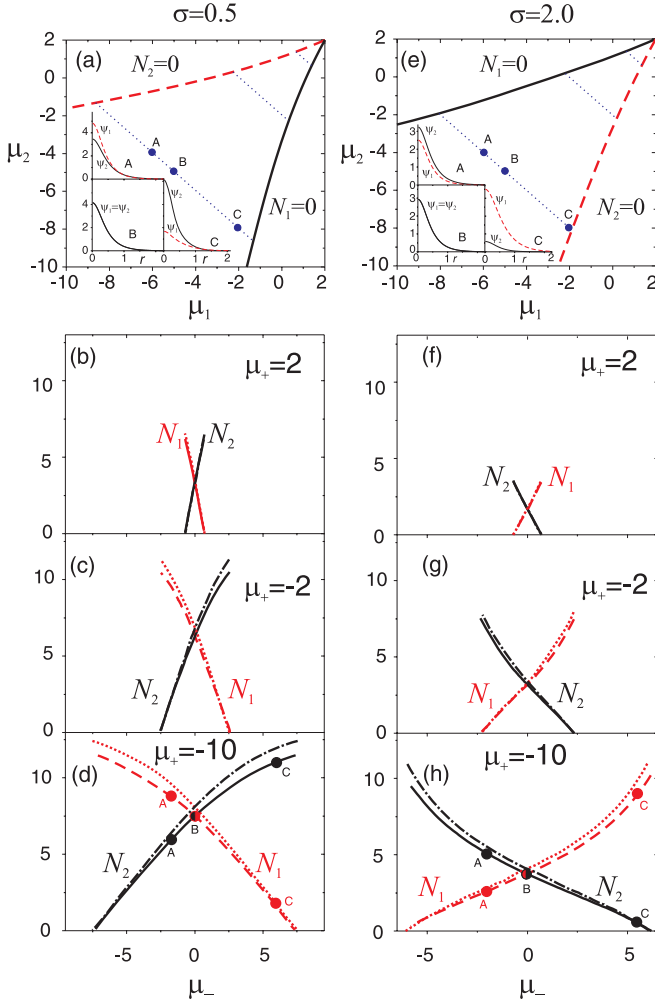
FIG. 1. (Color online) (a) and (e) Existence region for vector solitons in the (μ_1, μ_2) plane for $\sigma = 0.5$ and 2.0. Insets: examples for radial profiles $\psi_1(r)$ (red dashed line) and $\psi_2(r)$ (black solid line) at points A, B, and C in the (μ_1, μ_2) plane; $A = (-6, -4)$, $B = (-5, -5)$, $C = (-2, -8)$. (b)–(d) and (f)–(h) The number of atoms N_1 (red dashed line for numerical, red dotted line for variational results) and N_2 (black solid line for numerical results, black dashed-dotted line for variational results). The number of atoms are plotted as functions of the difference $\mu_- = \mu_1 - \mu_2$ at fixed total chemical potential $\mu_+ = \mu_1 + \mu_2$. The dotted straight lines in (a) and (e) correspond to the μ_+ of the particle number profiles given in (b)–(d) and (f)–(g), respectively.

other component vanishes. As expected, these curves merge at the point $\mu_1 = \mu_2 = 2$ where both components vanish. With increasing interaction strength σ the region of existence for vector solitons gradually shrinks, and at $\sigma = 1$ the boundaries degenerate to a straight line. Indeed, only pairs of identical solitons with equal chemical potentials exist if $\sigma = 1$. For $\sigma > 1$, where intercomponent interactions dominate over intracomponent interactions, the region of existence for vector solitons grows again. With respect to the case $\sigma < 1$ the boundary lines of the existence region swap around [compare Figs. 1(a) and 1(e)].

As is seen from Fig. 1, the number of particles $N_j(\mu_-)$ reaches its maximum value $N_{j\,\text{max}}$ at the boundary of the

existence domain where the other component N_{3-j} vanishes. For decreasing total chemical potential μ_+, $N_{j\,\text{max}}$ increases towards $N_{\text{cr}} = 11.68$ for numerical solutions and $N_{\text{cr}} = 4\pi$ for the variational trial functions Eq. (7). In order to relate these critical particle numbers to experimentally relevant parameters we determine the normalization of the 3D wave function $\langle \Psi | \Psi \rangle = N^{(3\text{D})}$, from which one obtains the number of trapped atoms in a disk-shaped BEC: $N_{\text{cr}}^{(3\text{D})} \approx 0.1\beta N_{\text{cr}}$, where $\beta = l_z / |a_{ii}|$ is the ratio of longitudinal oscillator length $l_z = \sqrt{\hbar/(M\omega_z)}$ to the scattering length between atoms of the same sort.

The remarkably different behavior of the functions $N_j(\mu_-)$ for weak or strong intercomponent interactions is evident from a comparison of Figs. 1(d) and 1(h). In the first case $(0 < \sigma < 1)$ the number of atoms saturates at $N_{j\,\text{max}} \leqslant N_{\text{cr}}$. In the second case $(\sigma > 1)$ the number of atoms decays rapidly from $N_{j\,\text{max}} \leqslant N_{\text{cr}}$ at one boundary to zero at the other boundary of the existence domain. It is easy to verify that for the case $\sigma > 1$ the sum of the number of particles in each component is always less than the critical value N_{cr}. For weak intercomponent interactions $(0 < \sigma < 1)$ we may find $N_1 + N_2 > N_{\text{cr}}$.

In summary, if intercomponent as well as intracomponent interactions are attractive, then both solitonic components are localized at the bottom of the potential trap, and the number of atoms in each component is subcritical. These facts change dramatically for repulsive intercomponent interactions, which we discuss next.

B. Repulsive intercomponent interactions ($\sigma < 0$)

To gain insight into the properties of the fundamental vector solitons with intercomponent repulsion we first present the results of a variational analysis. They provide a rather complete overview of the steady states which correspond to stationary points of the total energy Eq. (4) at a fixed number of atoms in each component.

Minima of the total energy at a given number of atoms can be attained for two different types of the solutions. The first type we call "bell shaped" since the density distribution of both components looks Gaussian-like. To stabilize such a "miscible" configuration for negative σ, the particle number in each component must increase with respect to the previously discussed case $\sigma > 0$ in order to compensate for the additional intercomponent repulsion by increased intracomponent attraction. Solutions of the second type will be referred to as "phase-separated" or "immiscible." These solutions minimize the "component-overlapping" part of the total energy [the last term in Eq. (4)] by substantially changing the shape of the density distributions. One component is pushed outward and forms a ringlike shell, while the other component is noticeably compressed—it has a higher peak density and narrower width than its noninteracting counterpart. The "immiscible" states are typical for BECs with both repulsive intra- and intercomponent interactions [30–35]. A simple condition for phase separation can be obtained by minimizing the interaction energy [36]: $g_{12}^2 > g_{11}g_{22}$; i.e., the intercomponent repulsion dominates. An accurate analysis of phase separation in repulsive BECs is given in Refs. [10,17]. If the interaction between atoms of the same

sort are attractive and the number of atoms in the solitonic components differ significantly, then a local-density depletion in the center of one component may appear for any strength of repulsive intercomponent interactions. Yet another notable feature of BECs with attractive intracomponent but repulsive intercomponent interactions is the possible coexistence of "miscible" and "immiscible" states for the same chemical potentials.

The simplest normalized trial function $\psi_j(r)$ supporting spatially separated components is given by the Ansatz

$$\psi_j(r) = A_j\left(1 + \delta_j \frac{r^2}{a_j^2}\right)e^{-\frac{1}{2}\frac{r^2}{a_j^2}}, \qquad (9)$$

where a_j is the effective width of component j of the soliton-soliton pair, and $A_j = \sqrt{N_j/\{\pi a_j^2[1 + 2\delta_j(1 + \delta_j)]\}}$. The parameter $\delta_j \geqslant 0$ introduces deviations from the Gaussian-like shape of the soliton. If $\delta_j > 1/2$, the density distribution has a local minimum at the bottom of the external potential trap. Evidently only one of the two BEC components is forced outward by repulsive intercomponent interactions. Consequently, δ_2 may be set to zero without loss of generality and we need to determine only three variational parameters: a_1, a_2, and $\delta = \delta_1$. Variational results for the number of atoms as functions of the chemical potential difference $\mu_- = \mu_1 - \mu_2$ are shown in Fig. 2.

Let us first discuss the properties of the "bell-shaped" solutions with $\delta = 0$. These solutions are presented in Fig. 2 by
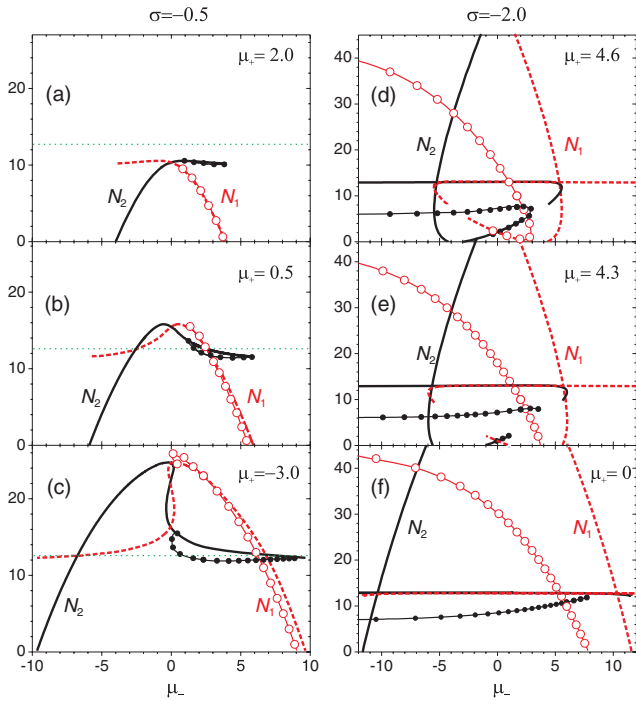
the red dashed curves for N_1 and by the solid black line for N_2. As they should, solutions with the same chemical potential and same number of atoms only exist for $\mu_+ < 4$ if $-1 < \sigma < 0$ and for $\mu_+ > 4$ if $\sigma < -1$. For $-1 < \sigma < 0$, the existence domain of vector solitons is bounded in the (μ_1, μ_2) plane like in the case $\sigma > 0$.

However, if intercomponent repulsion dominates over intracomponent attraction ($\sigma < -1$) "bell-shaped" solutions exist for any chemical potential. It is remarkable that even at $\mu_- = 0$ the solitonic components differ essentially from each other for $\mu_+ < 4$ [see Fig. 2(f)], but for $\mu_+ > 4$ there appears an additional branch of solutions that share the same profile at $\mu_- = 0$ [see Figs. 2(d) and 2(e)]. The gap between these two branches gradually disappears when μ_+ increases [compare Figs. 2(e) and 2(d)]. For relatively weak intercomponent interactions ($-1 < \sigma < 0$) and decreasing μ_+ the absolute value of the derivatives $|\partial N_j/\partial \mu_j|$ grows rapidly in the vicinity of the intersection point. Furthermore, it is interesting that in the profile for $N_j(\mu_-)$ a cusp appears for $N_j(0) > 16\pi/(3 + \sigma)$ provided that $-1 < \sigma < -1/3$. In this case two additional crossing points are observed at $\mu_1 = \mu_2$ [see Fig. 2(c)].

The properties of the second type of solutions ("phase-separated" states with $\delta > 0$), predicted by the variational method, are illustrated in Fig. 2 for $N_1(\mu_-)$ by red lines with open circles and for $N_2(\mu_-)$ by black curves with filled dots. Recall that we show only solutions with $\delta_1 = \delta$ and $\delta_2 = 0$ but the rest of the solutions can be easily constructed using the corresponding symmetry. The parameter δ describing the deviation of the radial profile from the Gaussian-like shape is given in Fig. 3. Here, $\delta(\mu_-)$ is shown for the same values of σ and μ_+ as in Fig. 2. As is seen from Fig. 3 the variational parameter δ reaches zero at some value of μ_-, where the two types of solutions $\delta > 0$ and $\delta = 0$ merge. Indeed this is also observed in Fig. 2 for solutions with $\mu_1 \approx \mu_2$.

The above-described features of phase-separated steady states obtained using the variational approach are supported by numerical simulations of Eq. (6). Note that only half of the phase-separated solutions are shown in Figs. 5(f)–5(h) to avoid confusion. The traces in these figures can easily be completed using the replacements $N_1 \rightarrow N_2$ and $\mu_- \rightarrow -\mu_-$. Unfortunately, our relaxation technique is not able to reproduce both types of solutions predicted by variational method for repulsive intercomponent interactions since the "bell-shaped"
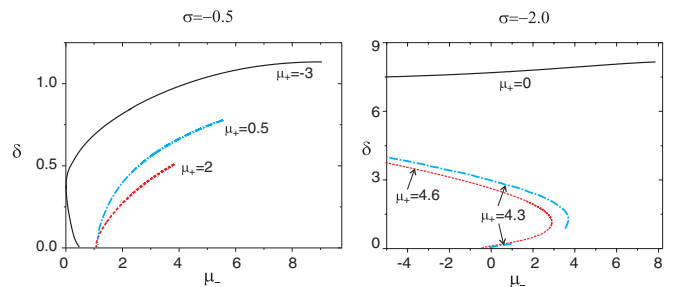

FIG. 2. (Color online) Variational results for $\sigma = -0.5$ [(a)–(c)] and -2.0 [(d)–(f)]. Shown are the number of atoms N_1 (red dashed curve for solutions with $\delta = 0$, red curves with open circles for solution with $\delta > 0$) and N_2 (solid black curves for solutions with $\delta = 0$ and black curves with filled dots for solutions with $\delta > 0$) as the functions of $\mu_- = \mu_1 - \mu_2$ at different values of the total chemical potential $\mu_+ = \mu_1 + \mu_2$. Green dotted line: $N = N_{\mathrm{cr}} = 4\pi$.

FIG. 3. (Color online) Variational parameter δ as a function of $\mu_- = \mu_1 - \mu_2$ for different values of the total chemical potential $\mu_+ = \mu_1 + \mu_2$.
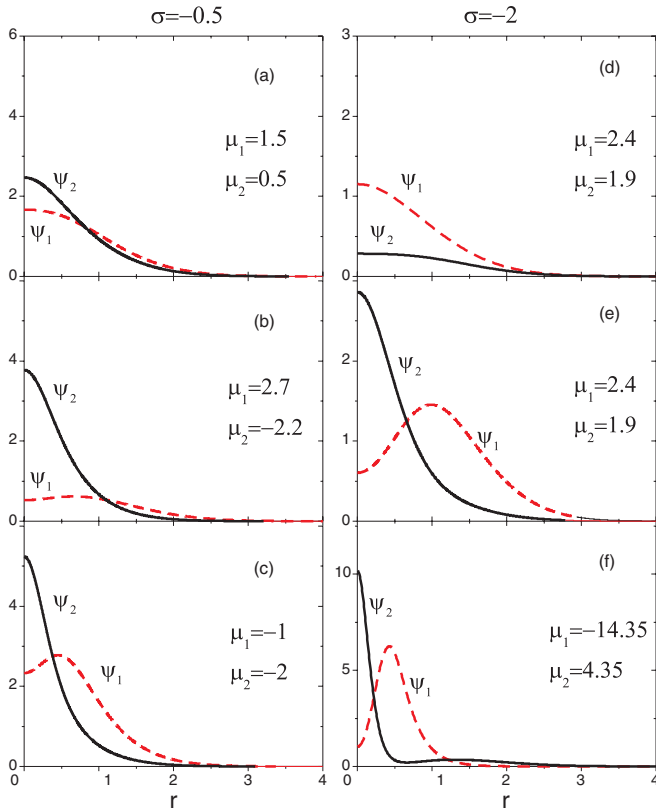
FIG. 4. (Color online) Examples of radial profiles ψ_1 (red dashed curves) and ψ_2 (black solid curves) for $\sigma = -0.5$ and -2.0 found numerically.

FIG. 5. (Color online) Top: Stability region in the (μ_1, μ_2) plane (green) as obtained by numerical simulations: (a) $\sigma = -0.5$, (b) $\sigma = -2.0$. Bottom: Number of atoms N_1 (red dashed curves) and N_2 (black solid curves) as a function of the chemical potential difference $\mu_- = \mu_1 - \mu_2$ at fixed total chemical potential $\mu_+ = \mu_1 + \mu_2$ obtained numerically: (c)–(e) $\sigma = -0.5$, (f)–(h) $\sigma = -2.0$. The dotted straight lines in (a) and (e) correspond to the μ_+ of the particle number profiles given in (b)–(d) and (f)–(g), respectively.

solutions (with $\delta_1 = \delta_2 = 0$) usually have higher energies than the phase-separated solutions at the same chemical potential. That is why our numerical procedure rather converges to the "phase-separated" solutions or to scalar solitons. Therefore, our analysis of the steady states with $\delta_1 = \delta_2 = 0$ is limited to the variational method.

Typical radial profiles found numerically are shown in Fig. 4. Generally, the numerical results are found to be in good agreement with the variational predictions for the "phase-separated" solutions. One expects, however, differences between numerical and variational results for solutions with a very dense ring-shaped component. Indeed, a ring component with large amplitude could push away the atoms at the periphery of the core component. Consequently, an additional outer ring should be observed in the density distribution of the core component. Moreover, if the number of atoms increases even more, then more and more rings should appear in both solitonic components. Actually, an additional outer ring is seen for $\psi_2(r)$ in Fig. 4(f), and such a modification of the core component explains the nonmonotonic behavior of the diagrams $N_2(\mu_-)$ at negative μ_- in Figs. 5(f)–5(h).

IV. STABILITY ANALYSIS

A few general conclusions concerning stability follow from our variational analysis. In fact, it is easy to find a *sufficient* condition for stability against radially symmetric collapse: if both solitonic components satisfy the condition $N_j < N_{\mathrm{cr}}$,
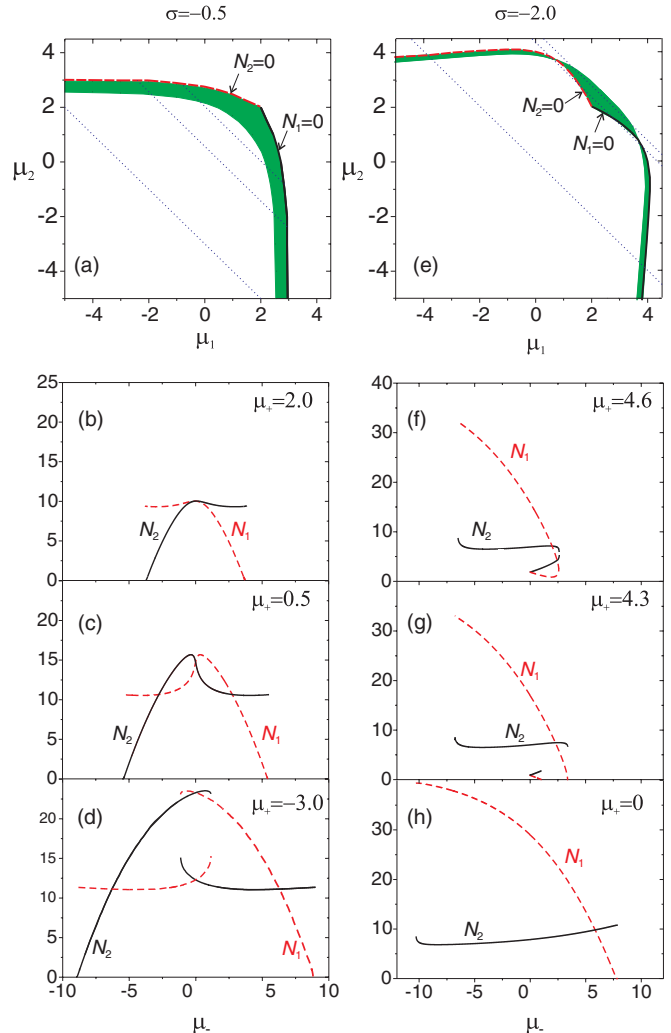
then the stationary solutions are expected to be stable since they correspond to the minimum of the total energy. As was shown in the previous section, for attractive intercomponent interactions ($\sigma > 0$) the particle numbers in both solitonic components are always below the critical value and, therefore, the vector solitons should be stable in this case.

For $\sigma < 0$, the variational analysis predicts the existence of two types of stationary solutions: "phase-separated" states and colocated "bell-shaped" states with different stability properties. The solutions with $\delta_1 = \delta_2 = 0$ should be stable provided $N_1 < N_{\mathrm{cr}}$ and $N_2 < N_{\mathrm{cr}}$. At the same time, the phase-separated states are predicted to be stable against collapse even if the ring component j (with $\delta_j > 0$) is supercritical provided that the bell-shaped component (with $\delta_{3-j} = 0$) consists of a subcritical number of particles.
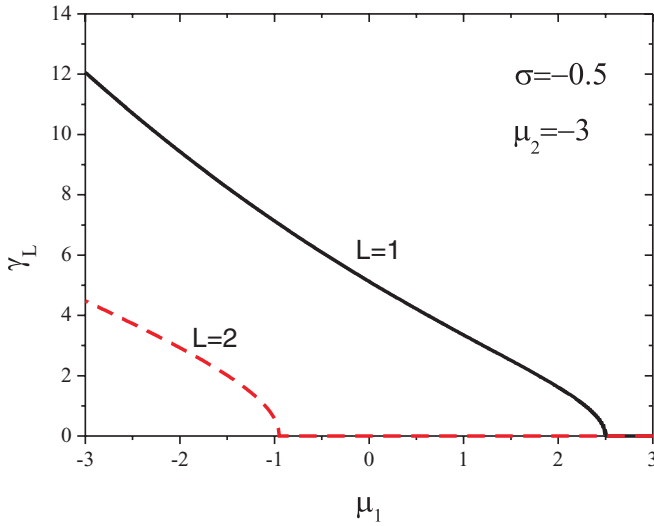
FIG. 6. (Color online) Maximum growth rates as a function of μ_1 at fixed μ_2. Note that all growth rates vanish above some threshold value of μ_1.
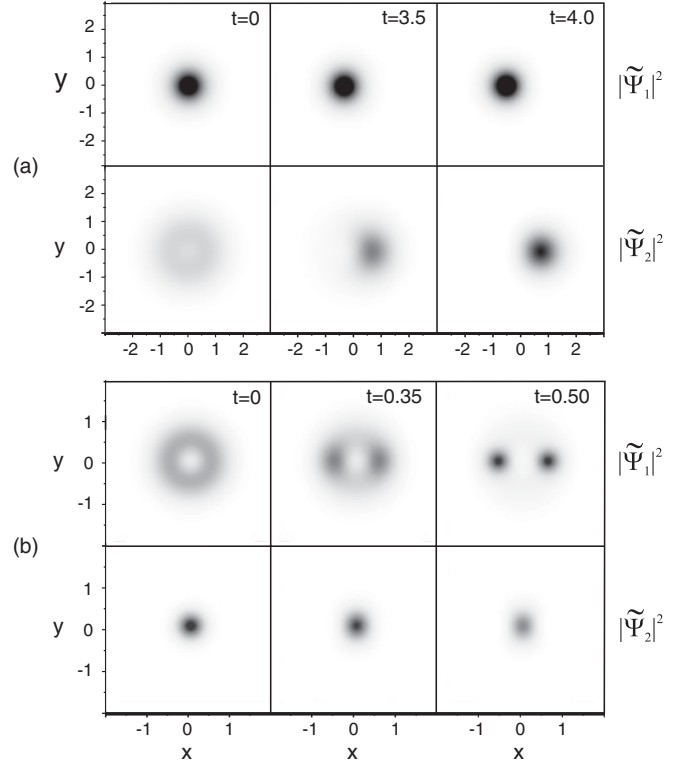

FIG. 7. (Color online) Time evolution of the density distributions $|\tilde{\Psi}_1|^2$ (upper rows) and $|\tilde{\Psi}_2|^2$ (lower rows) of perturbed vector solitons for (a) $\sigma = -0.5$, $\mu_1 = -1.5$, $\mu_2 = 2$ and (b) $\sigma = -0.8$, $\mu_1 = -5$, $\mu_2 = -5$.

It is clear that a radially symmetric variational analysis does not provide any information about the stability with respect to azimuthal perturbations. This question may be addressed by numerical simulations as discussed below. In contrast to the results of the variational analysis our numerical simulations predict the phase-separated states to be unstable against collapse even if only one component has a number of particles above the critical value N_{cr}. Note that numerical time evolution of the variational Ansatz for the steady states with $\delta_1 = \delta_2 = 0$ confirmed their stability only in the region where these solutions practically merge with the second solitonic branch [see Figs. 2, 3, and 5].

The stability of the stationary solutions with respect to azimuthal symmetry-breaking perturbations was investigated by a linear stability analysis. We write the order parameter of the two-component BEC in the form $\tilde{\Psi}_j(r,t) = [\psi_j(r) + \varepsilon_j(r,t)]e^{-\mu_j t}$ with a small perturbation $\varepsilon_j(r,t) = u_j(r)e^{i\omega t + iL\varphi} + v_j^*(r)e^{-i\omega^* t - iL\varphi}$ and insert it into Eq. (2). We linearized the resulting equations with respect to ε and solved the resulting eigenvalue problem for ω. Solutions exhibiting an imaginary part would indicate instability.

We find that $\gamma_L = \text{Im}(\omega)$ are identically zero for all L if the intercomponent interaction is attractive. If it is repulsive the azimuthal modes $L = 1$ and 2 may be unstable. A typical example for a maximum growth rate γ_L as a function of the chemical potential μ_1 at fixed μ_2 is shown in Fig. 6. The unstable modes with $\gamma_L \neq 0$ have eigenfrequencies with vanishing real part: $\text{Re}(\omega) = 0$; i.e., the azimuthal instabilities that may appear for the case of repulsive intercomponent interactions are always aperiodic. The evolution scenario that appears as a result of a developed azimuthal instability is discussed below in more detail. But it is clear that an instability of the $L = 1$ mode leads to relative motion of the BEC components, while the unstable $L = 2$ mode is expected to split the ring-shape component into two filaments. Note that above some threshold the growth rates vanish. It is important to realize that the mode $L = 1$ has a much wider instability region than $L = 2$, and that the growth rates of the mode

$L = 2$ are smaller than those of the mode $L = 1$. Therefore, the $L = 1$ modes are most dangerously influencing the stability of repulsively interacting solitons.

The predictions of the variational analysis and the results of the linear stability analysis have been tested by numerical experiments of the time evolution of the perturbed vector solitons. For the numerical solution of the time-dependent GPEs (2) a standard split-step Fourier-transform method (see, e.g., Ref. [37]) has been used. While vector solitons with attractive intercomponent interactions are confirmed to be stable over the full existence domain, repulsive intercomponent interactions lead to various instabilities. Typical examples for unstable dynamics are given in Fig. 7.

We found that, if at least one solitonic component contains an overcritical number of atoms, then the stronger component finally collapses. However, we do not see a collapse if both solitonic components are subcritical. Obviously, the potential trap prevents the unlimited expansion of the BEC. Furthermore, the final collapse is not possible if the number of atoms in both components is subcritical, so as the result of symmetry-breaking instability we see a contraction and relative motion of the two solitonic components. Oscillations between such a quasicollapse and an asymmetric state are shown in Fig. 7(a) for times $t = 3.5$ and 4.0. Here, both solitonic components are subcritical, and the growth rate for the $L = 1$ mode is nonvanishing.

The growth of the $L = 2$ mode leads to the decay of the shell component of the soliton into two filaments. In the

beginning, two humps and two holes appear in the ring, and the inner component rapidly leaks through these hollows into a ring-shaped "well." Repulsive intercomponent interactions between the ring-shaped component and the leaking inner component lead to an increase of the hollows and finally the ring breaks up into two separate parts as seen in Fig. 7(b). Note that the dynamics of the unstable trapped two-component BEC is similar to the evolution of vector solitons reported in Ref. [27] within a similar model but without external trapping potential. The most outstanding feature of trapped matter wave vector solitons is the fact that they can be completely stabilized even for strong repulsive intercomponent interactions. We show the stability region in green color in the (μ_1, μ_2) plane for weak ($\sigma = -0.5$) and strong ($\sigma = -2.0$) intercomponent repulsive interactions in Figs. 5(a) and 5(e).

V. SUMMARY AND CONCLUSIONS

Fundamental 2D soliton-soliton pairs are investigated in two-component BECs with attractive intracomponent interactions. General properties of vector solitons and their stability are studied variationally and numerically for both attractive and repulsive intercomponent interactions. We found different types of soliton-soliton pairs including phase-separated pairs where one component is pushed outward and forms a ringlike shell and the other component is compressed due to repulsive intercomponent interactions. It turns out that for some values of

the chemical potentials phase-separated steady states coexist with collocated states characterized by bell-shaped density distributions in both components.

We performed a linear stability analysis of small azimuthal perturbations and checked these results by an extensive series of numerical simulations. For attractive intercomponent interactions matter wave bright vector solitons are demonstrated to be stable throughout the existence domain. For BEC components which repel each other various unstable evolution scenarios including collapse and azimuthal symmetry-breaking instabilities are observed. The instabilities, as a rule, lead either to separation of the condensed phases and then a collapse of the stronger supercritical ($N > N_{cr}$) component or a periodic relative motion of the subcritical ($N < N_{cr}$) solitonic components backward and forward near the bottom of the trapping potential. Nevertheless, there are conditions where complete stabilization of vector solitons is observed even in the case of repulsive intercomponent interactions.

[1] K. T. Kapale and J. P. Dowling, Phys. Rev. Lett. **95**, 173601 (2005).

[2] M. E. Zawadzki, P. F. Griffin, E. Riis, and A. S. Arnold, Phys. Rev. A **81**, 043608 (2010).

[3] T. van Zoest *et al.*, Science **328**, 1540 (2010).

[4] S. G. Bhongale and E. Timmermans, Phys. Rev. Lett. **100**, 185301 (2008).

[5] P. G. Kevrekidis, H. E. Nistazakis, D. J. Frantzeskakis, B. A. Malomed, and R. Carretero-González, Eur. Phys. J. D **28**, 181 (2004).

[6] P. Öhberg and L. Santos, Phys. Rev. Lett. **86**, 2918 (2001).

[7] K. Kasamatsu and M. Tsubota, Phys. Rev. Lett. **93**, 100402 (2004).

[8] P. G. Kevrekidis, H. Susanto, R. Carretero-González, B. A. Malomed, and D. J. Frantzeskakis, Phys. Rev. E **72**, 066604 (2005).

[9] V. M. Pérez-García and J. B. Beitia, Phys. Rev. A **72**, 033620 (2005).

[10] M. Trippenbach, K. Góral, K. Rzazewski, B. Malomed, and Y. B. Band, J. Phys. B **33**, 4017 (2000).

[11] D. V. Skryabin, Phys. Rev. A **63**, 013602 (2000).

[12] J. J. García-Ripoll and V. M. Pérez-García, Phys. Rev. Lett. **84**, 4264 (2000).

[13] V. M. Pérez-García and J. J. García-Ripoll, Phys. Rev. A **62**, 033601 (2000).

[14] S. K. Adhikari, Phys. Lett. A **346**, 179 (2005).

[15] G. Thalhammer, G. Barontini, L. De Sarlo, J. Catani, F. Minardi, and M. Inguscio, Phys. Rev. Lett. **100**, 210402 (2008).

[16] S. B. Papp, J. M. Pino, and C. E. Wieman, Phys. Rev. Lett. **101**, 040402 (2008).

[17] L. Wen, W. M. Liu, Y. Cai, J. M. Zhang, and J. Hu, Phys. Rev. A **85**, 043602 (2012).

[18] M. Brtka, A. Gammal, and B. A. Malomed, Phys. Rev. A **82**, 053610 (2010).

[19] G. Filatrella, B. A. Malomed, and L. Salasnich, Phys. Rev. A **79**, 045602 (2009).

[20] M. Matuszewski, B. A. Malomed, and M. Trippenbach, Phys. Rev. A **76**, 043826 (2007).

[21] P. G. Kevrekidis, H. E. Nistazakis, D. J. Frantzeskakis, B. A. Malomed, and R. Carretero-González, Eur. Phys. J. D **28**, 181 (2004).

[22] L. Salasnich and B. A. Malomed, Phys. Rev. A **74**, 053610 (2006).

[23] R. Shibato, T. Nishimura, T. Watanabe, and T. Suzuki, Phys. Rev. A **84**, 043627 (2011).

[24] P. G. Kevrekidis, D. J. Frantzeskakis, and R. Carretero-Gonzalez, *Emergent Nonlinear Phenomena in Bose-Einstein Condensates* (Springer, Berlin, 2008).

[25] L. Bergé, T. J. Alexander, and Y. S. Kivshar, Phys. Rev. A **62**, 023607 (2000).

[26] A. I. Yakimenko, Y. A. Zaliznyak, and V. M. Lashkin, Phys. Rev. A **79**, 043629 (2009).

[27] A. I. Yakimenko, O. O. Prikhodko, and S. I. Vilchynskyi, Phys. Rev. E **82**, 016605 (2010).

[28] T. J. Alexander and L. Bergé, Phys. Rev. E **65**, 026611 (2002).

[29] V. I. Petviashvili, Soviet Journal of Plasma Physics **2**, 469 (1976).

[30] T.-L. Ho and V. B. Shenoy, Phys. Rev. Lett. **77**, 3276 (1996).
[31] H. Pu and N. P. Bigelow, Phys. Rev. Lett. **80**, 1130 (1998).
[32] H. Pu and N. P. Bigelow, Phys. Rev. Lett. **80**, 1134 (1998).
[33] X. Liu, H. Pu, B. Xiong, W. M. Liu, and J. Gong, Phys. Rev. A **79**, 013423 (2009).
[34] S. K. Adhikari, Phys. Rev. E **63**, 056704 (2001).

[35] L. Zhou, J. Qian, H. Pu, W. Zhang, and H. Y. Ling, Phys. Rev. A **78**, 053612 (2008).
[36] C. J. Pethick and H. Smith, *Bose-Einstein Condensation in Dilute Gases* (Cambridge University Press, Cambridge, 2002).
[37] G. Agrawal, *Nonlinear Fiber Optics* (Academic Press, London, 2006).